Powder Technology 448 (2024) 120299

Contents lists available at ScienceDirect

Powder Technology

journal homepage: www.journals.elsevier.com/powder-technology

CFD-DEM modeling for optimized liquid distribution in fluidized bed spray granulation

Maike Orth [a,*,1], Aitor Atxutegi [a,*,1], Matthias Börner [b], Swantje Pietsch-Braune [a], Stefan Heinrich [a]

[a] Institute of Solids Process Engineering and Particle Technology, Hamburg University of Technology, Denickestraße 15, Hamburg, 21073, Germany
[b] Hüttlin GmbH, A Syntegon Company, Hohe-Flum-Straße 42, Schopfheim, 79650, Germany

HIGHLIGHTS

- A novel fluidized bed granulator geometry was investigated by means of CFD-DEM simulations.
- Locally resolved droplet deposition rate as well as droplet fates were analyzed.
- Reactor geometry significantly influences liquid distribution.
- Detailed information of the deposition can help to detect local overwetting.

GRAPHICAL ABSTRACT

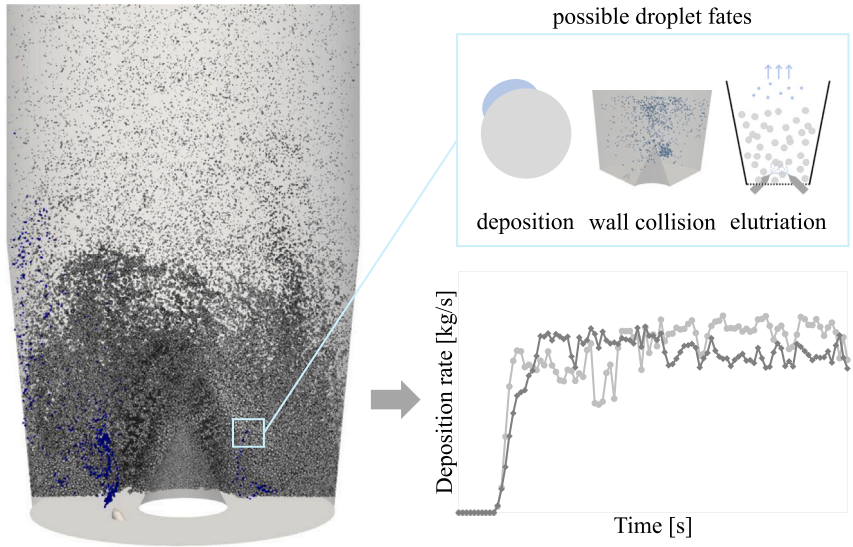

ARTICLE INFO

Keywords:
CFD-DEM simulation
Fluidized bed spray granulation
Liquid distribution
Bottom-spray
Tangential air inlet

ABSTRACT

In this work, CFD-DEM simulations of two different fluidized bed granulator geometries were performed, aiming to provide an insight into how the injected liquid behaves within the particle bed and thus an overall better understanding of the granulation process itself. Simulation results were evaluated regarding the fate of sprayed droplets, e.g. deposition on a particle, elutriation from fluidized bed, or collision with apparatus walls. For the deposited droplets, the particle–droplet collisions were tracked in order to obtain a locally resolved deposition rate. Spray parameters as well as geometric specifications of the nozzle setup were varied, investigating a broad range of different process conditions. By optimizing apparatus design, especially the air inlet, an even distribution of the liquid droplets within the fluidized bed and overall higher deposition rate can be achieved and a stable steady state with a well-defined spray zone is reached within a broad range of varied spray parameters.

* Corresponding authors.
E-mail addresses: maike.orth@tuhh.de (M. Orth), aitor.achutegui@tuhh.de (A. Atxutegi).
[1] Both authors contributed equally to this paper.

https://doi.org/10.1016/j.powtec.2024.120299
Received 23 July 2024; Received in revised form 11 September 2024; Accepted 16 September 2024
Available online 19 September 2024

1. Introduction

1.1. Fluidized bed spray granulation

Fluidized bed spray granulation is an important and widespread technology for the production of high-quality particulate solids. The process has been applied for more than 60 years and ever since the fields of application have expanded considerably [1]. Nowadays, spray granulation is applied in various industries, including pharmaceutical, chemical, and food industry, to produce a broad variety of products. For some of these products, such as pharmaceuticals, the fluidized bed process and the excellent mixing associated with it are used to obtain granules with a precise and evenly distributed dose of an active ingredient. For instant food powders, a fast and complete reconstitution is often desirable in addition to a dust-free and free-flowing behavior while handling the particles [2,3].

Granulation generally refers to size enlargement processes based on different growth mechanisms. In wet granulation, particle growth is induced by the injection of a liquid and subsequent layering or bridge formation. Specific to the field of application, the term granulation is used for both mechanisms. For a clear distinction, coating and agglomeration can be distinguished [4,5]. In coating, the liquid droplets are deposited on the particles, spreading of the surface before being dried by the hot fluidization gas and thus forming a solid layer around the core particle [6]. In contrast, agglomeration describes the formation of stable particle clusters from primary particles and if necessary a binder. When two wet particles collide, a liquid bridge is formed, which binds the particles together due to viscous and capillary forces. By subsequent drying, a solid bridge is created. Due to repeated wet particle collisions and bridge formation, agglomerates grow further [5]. In this work, fluidized bed agglomeration is the particle growth mechanism of interest.

Structure and further desired agglomerate properties can be influenced by the materials used as well as the design of the process and equipment. These influences were investigated in several experimental studies, such as those by Hemati et al. [7], Pont et al. [8], and Rajniak et al. [9], who analyze the effect of spray solution properties on agglomerate growth. Further works, e.g. by Bouffard et al. [10], Dadkhah and Tsotsas [11], Lipps and Sakr [12], Saleh et al. [13], and Vengateson and Mohan [14], are concerned with the influence of process parameters on the agglomeration process and the characteristics of the final product.

1.2. Types of equipment

Nozzles with the purpose of injecting a liquid into a fluidized bed can be installed in different positions, including top-spray, bottom-spray, and tangential-spray. The top-spray configuration, where the nozzle is positioned above the particle bed spraying downwards, is the most commonly used setup. While the large particle bed surface available to the spray promotes the deposition of droplets on the fluidized particles, the strongly fluctuating flight distance and time of the droplets increase the risk of a droplet evaporating before it collides with a particle [15–17]. In addition, the distribution of liquid between the individual particles might not be completely uniform.

In bottom-spray configuration, the nozzle is installed at the bottom of the fluidized bed, most commonly at the center of the distributor plate, and covered by particles. The nozzle is directed upwards, so that liquid is sprayed co-current to the fluidization air. Compared to top-spray, the droplet flight times and distances are significantly shorter, reducing the risk of spray drying the droplets. However, wetting might again be inhomogeneous due to the random particle motion within the fluidized bed, which can cause overwetting and subsequent lump formation or even bed collapse [15].

In order to ameliorate the liquid distribution in bottom-spray processes, the equipment can be modified by installing additional components or changing nozzle direction and position within the bottom of the bed. A setup that is commonly used for coating of pharmaceuticals is a Wurster coater, which consists of a vertical draft tube placed centrally above the distributor and a modified distributor with larger orifices in the area underneath the tube [15,18,19]. Due to the enhanced gas velocity at the center, a structured, circulating particle motion is created and the fluidized bed is separated into a wetting and a drying zone. Further alternative setups consist of several inclined nozzles installed in bottom-spray configuration, such as the geometry investigated in this study, as explained in Section 2 in more detail.

1.3. Numerical investigations

As mentioned above, several experimental studies have shown that process setup and conditions significantly influence agglomerate properties and quality. However, it remains challenging to obtain insights into the microscopic processes occurring within the fluidized bed such as how particles move within the bed, where particle–droplet collisions take place, and how efficient the injected liquid is used in agglomerate formation. Furthermore, there is a lack of works investigating the effects of equipment modifications on the agglomeration process since changes in the reactor geometry are often work- and cost-intensive. The design of fluidized bed equipment as well as the agglomeration process itself are still often developed empirically and are based on experience rather than a comprehensive understanding of the physical and chemical phenomena happening within the three-phase process [15,20,21]. Therefore, difficulties in predicting process behavior for new materials and scales, while keeping good product quality, arise [5]. To overcome both of these challenges, investigating micro processes and varying equipment geometry in a simulation environment provides a powerful tool for the analysis of fluidized bed agglomeration.

Cameron et al. [22] offer an extensive review on the modeling of wet agglomeration processes, such as fluidized bed agglomeration, which highlights population balances as the most used simulation approach. However, the growing need for micro-scale investigations, realized by approaches such as a coupling of computational fluid dynamics (CFD) and the discrete element method (DEM), is also mentioned. A more recent review by Singh et al. [23] discusses simulation of pharmaceutical granulation processes by population balance modeling, data-driven models, and DEM. In general, CFD-DEM is a Euler–Lagrange approach, in which the fluid phase is described as a continuous phase by solving the Navier–Stokes equations and the particles are tracked individually by solving Newton's equations of motion [24]. Possibilities and limits of this simulation approach in the context of process engineering were summarized by Kieckhefen et al. [25].

Different approaches have been used to integrate a liquid phase into CFD-DEM simulations. Goldschmidt et al. [26] included liquid droplets in form of additional discrete elements to simulate particle growth due to interaction between particles and droplets. Simplifications made in this study include the assumption of a two-dimensional fluidized bed as well as the limitation to 50,000 initial particles and large droplet diameters. Link et al. [27] investigated a simplified pseudo-two-dimensional spouted bed with droplet injection, where mass and momentum of a droplet are directly transferred to the particle after a collision. The model was later extended by van Buijtenen et al. [28] and Sutkar et al. [29]. Kafui and Thornton [30] described the agglomeration process by including a contact model based on surface energy into their CFD-DEM simulations. Fries et al. [31] developed a model for a fluidized bed granulator by combining gas and particle dynamics with a particle wetting model that calculates the residence time of the particles in a conical spray zone to estimate the homogeneity of the liquid distribution based on the droplet deposition analysis [27]. The model was applied to a top-spray fluidized bed and a Wurster coater. In follow-up studies, CFD-DEM simulations including this model were used to monitor the moisture content and temperature of individual particles as well as the temperature and humidity of the fluidization

gas [32] and to calculate agglomeration probability, breakage, and growth rate [33]. However, no individual droplets were tracked in these studies. Börner et al. [34] applied a scaling approach based on similarity models to investigate residence time distribution in the spray and drying zone of a top-spray fluidized bed. In order to predict product properties from simulations, Kieckhefen [35] implemented a full-physics CFD-DEM solver to simulate fluidized bed spray granulation, which is capable of describing particle wetting due to the flow of droplets in the gas phase.

Liquid injection and distribution are among the most critical parameters in fluidized bed agglomeration, since an effective and uniform wetting of particles is essential to process efficiency and product quality. Over the last few years, continuous progress has been made in the application of the coupled CFD-DEM approach to physically accurately describe fluidized bed processes with liquid injection, as more aspects relevant to different applications are considered. However, the exact locations, where droplet deposition occurs in the particle bed, and how this is affected by spray parameters is yet to be investigated. Therefore, this study aims to further ameliorate the understanding of fluidized bed spray agglomeration by analyzing the local droplet deposition.

A novel fluidized bed geometry with a tangential gas inlet and two inclined nozzles in bottom-spray configuration was investigated by means of unresolved CFD-DEM simulations using the solver developed in [35]. To evaluate the liquid distribution, the droplet deposition throughout the particle bed was tracked. Since generally, various process conditions might be applied in agglomeration, depending on application and materials used, spray parameters were varied to analyze their influence on the droplet distribution. Furthermore, the simulation allows to easily test equipment modifications. Thus, the position of the bottom-spray nozzles relative to the gas inlet as well as the inclination angle of the nozzle were changed to find the optimal setup for efficient liquid injection. Lastly, a comparison between the newly developed geometry and a commercially available fluidized bed reactor with a central gas inlet was made.

2. Fluidized bed setup

Two different laboratory scale fluidized bed setups were considered in this study, the commercially available *Solidlab 2* (Syntegon Technology, Germany) and a prototype developed at Syntegon Technology (Germany). Both reactor geometries are shown in Fig. 1. The *Solidlab 2* consists of a cylindrical process and expansion chamber with a diameter of 300 mm. After passing a 90° bend, the fluidization gas is entering the reactor through an inlet pipe with a diameter of 81 mm placed centrally below the distributor plate.

The *Diskjet* distributor is a stainless steel plate with gaps of 0.2 mm width and 10 – 40 mm length in radial direction, through which the gas flows into the particle bed. Due to a 45° inclination of the gaps, the gas exits the distributor plate in an oblique direction ensuring a homogeneous fluidization of particles. A cone with a diameter of 80 mm and height of 90 mm is positioned in the center of the plate. Two nozzles are placed in bottom spray configuration at 160 mm distance from one another. Both nozzles are inclined at 40° to the distributor pointing in opposite directions. Each nozzle is a three-fluid nozzle with one liquid opening and two gas slits, one for the spray gas to atomize the liquid and one for a protection gas to ensure the nozzle tip stays free of solid particles, respectively. While several different liquid inserts and air caps are available to vary the orifice size through which the phases are flowing out of the nozzle, in this study only a liquid insert with orifice size of 1.2 mm and an air cap with an inner diameter of 2.3 mm were considered.

In contrast to the *Solidlab 2* setup, the prototype geometry is composed of a conical process chamber and a cylindrical expansion region. At the gas inlet the diameter is 300 mm which expands to 350 mm at the top of the reactor. As distributor plate, the *Diskjet* is used as well in the prototype. To support the effect of the inclined gaps on the gas flow, a flat wind box with a tangential air inlet is installed below the distributor. Three different versions of the wind box were 3D printed to allow the variation of the inclination angle of the two bottom spray nozzles between 40, 50, and 60°.

Table 1
Mesh properties for CFD simulation.

Geometry	Minimum cell volume	Maximum cell volume	Number of cells
Prototype	$1.5 \cdot 10^{-11}$ m^3	$7.2 \cdot 10^{-7}$ m^3	331 238
Solidlab 2	$4.1 \cdot 10^{-13}$ m^3	$1.2 \cdot 10^{-5}$ m^3	133 113

3. Numerical simulations

To carry out simulations, the open source CFD software *OpenFOAM* [36] and the DEM tool *LIGGGHTS* [37] were coupled using *CFDEMcoupling* [38].

To avoid the simulation of the complex gas inlet and distributor plate, CFD simulations of the full prototype reactor geometry were conducted first to calculate the gas flow field in the wind box and through the distributor. In these simulations, the distributor was modeled as a *explicitPorositySource* to match the pressure drop measured in the experimental equipment as well as the direction, in which the gas passes through the gaps of the *Diskjet*. For the CFD-DEM simulations, a simplified geometry including only the area accessible for particles was used as depicted in Fig. 2. The velocity field just above the distributor plate obtained from the CFD simulation was then mapped on this volume as inlet condition. For both geometries, the minimum and maximum mesh cell size as well as the total number of cells is given in Table 1.

For the description of the gas phase, the Navier–Stokes equations are solved using the *cfdemSolverEvap* developed in [35]:

$$\frac{\partial \left(\alpha_f \mathbf{u}_f\right)}{\partial t} + \nabla \cdot \left(\alpha_f \mathbf{u}_f \mathbf{u}_f\right) = -\frac{\alpha_f}{\rho_f}\nabla p - \frac{1}{\rho_f}\boldsymbol{R}_{pf} + \nabla \cdot \left(\frac{\alpha_f}{\rho_f}\boldsymbol{\tau}\right), \tag{1}$$

$$\frac{\partial \alpha_f}{\partial t} + \nabla \cdot \left(\alpha_f \mathbf{u}_f\right) = 0, \tag{2}$$

with the volume fraction of the fluid α_f, the fluid density ρ_f, the fluid velocity $\mathbf{u}_f$, and the pressure p. $\boldsymbol{\tau}$ is the stress tensor, which can be calculated from the fluid velocity and viscosity and $\boldsymbol{R}_{pf}$ describes the momentum exchange between fluid and solid phase. The momentum exchange term consists of a momentum exchange coefficient $\boldsymbol{K}_{pf}$ as well as the fluid and averaged particle velocity. This coefficient contains the drag forces within a certain cell volume and is calculated using a drag model. In this work, the correlation by Beetstra et al. [39] was utilized. To calibrate the drag model, the minimum fluidization velocity of the bed material was experimentally determined via pressure drop measurements in a cylindrical fluidized bed and afterwards compared to simulations of the cylindrical setup.

On the DEM side, the Newtonian equations of motions are solved to determine particle dynamics:

$$m_i \ddot{x}_i = \sum_i F_i, \tag{3}$$

$$I_i \dot{\omega}_i = \sum_i M_i, \tag{4}$$

where m_i is the particle mass, x_i is the particle position, F_i are the forces acting on particle i, I_i is the moment of inertia, ω_i is the angular velocity, and M_i are the torques. The Hertz–Mindlin model was used to calculate contact forces [40]. Static and rolling friction coefficients for particle–particle and particle–wall contacts were calibrated based on shear cell as well as static and dynamic angle of repose experiments as proposed in [41].

In this study, these calibration experiments were carried out with lactose granules that are considered as a model material for a pharmaceutical agglomeration process. Furthermore, the mean size and

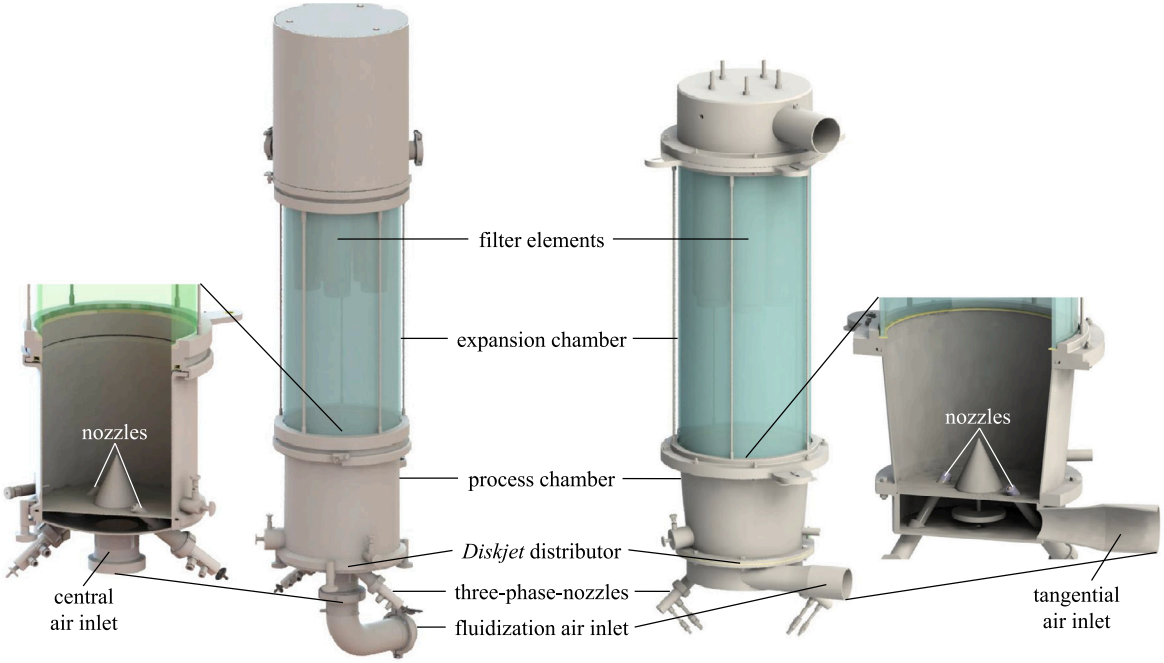

Fig. 1. Investigated fluidized bed setups (Syntegon Technology, Germany): *Solidlab 2* (left) and prototype (right).

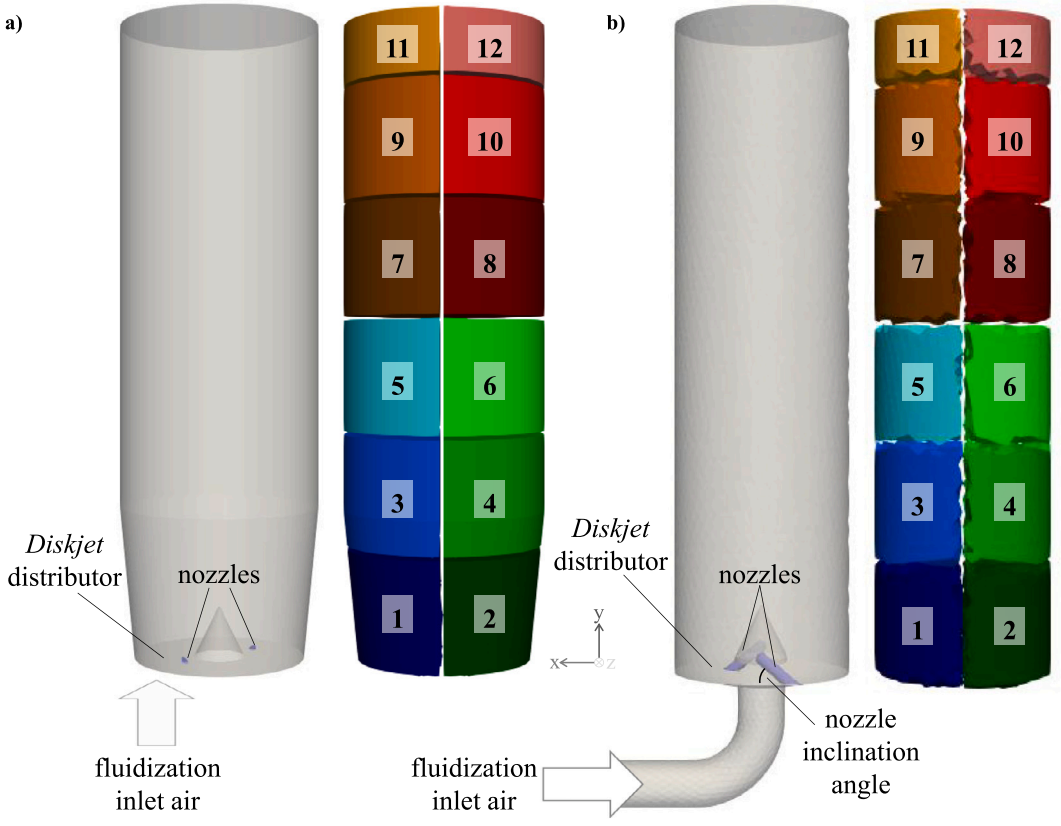

Fig. 2. Reactor volume for CFD-DEM simulations and division into segments for analysis of liquid distribution: (a) prototype, (b) *Solidlab 2*. Nozzles are highlighted in blue color.

Table 2
Material properties and model parameters used in simulations.

Parameter	Symbol	Value	Unit
CFD time step	Δt_{CFD}	$2 \cdot 10^{-4}$	s
DEM time step	Δt_{DEM}	10^{-5}	s
Scaling factor	δ	9.5	–
Number of particles	N_p	618 915	–
Particle diameter	d_p	500 – 2000	µm
Particle density	ρ_p	1551	kg/m^3
Young's modulus			
- Particle	Y_p	$2.5 \cdot 10^6$	Pa
- Wall	Y_w	10^7	Pa
Poisson ratio	ν	0.25	–
Restitution coefficient			
- Particle–particle	e_{p-p}	0.1	–
- Particle–wall	e_{p-w}	0.1	–
Friction coefficient			
- Particle–particle	$\mu_{fr,p-p}$	0.75	–
- Particle–wall	$\mu_{fr,p-w}$	0.8	–
Rolling friction coefficient			
- Particle–particle	$\mu_{rfr,p-p}$	0.825	–
- Particle–wall	$\mu_{rfr,p-w}$	0.8	–
Bed mass	m_{bed}	3	kg
Droplet diameter	$d_{droplet}$	1 – 80	µm

particle density were determined to be 160 µm and 1551.4 ± 9.9 kg/m^3. However, when using this particle size as reference, the number of particles in the considered fluidized beds would pose a challenge in terms of computational power. Therefore, in order to reduce computational cost, a coarse-graining approach was utilized. Coarse-graining reduces the number of tracked particles by combining several particles into parcels, which are enlarged by a factor δ:

$$\delta = \frac{d_{parcel}}{d_p}. \tag{5}$$

The number of particles is thereby decreased by δ^3 allowing for a bigger time step to be used in simulations. In this work, the coarse-graining approach according to Bierwisch et al. [42] was utilized.

As fluidization gas, air is assumed to enter the reactor at 80 °C. The injected liquid is modeled as Lagrangian parcels, which consist of several droplets. Once a particle–droplet collision occurs, the particle mass is recalculated and the interaction with other particles is adapted in dependence of the amount of water on the particle surface. As described in [43], droplet deposition was modeled using the filter correlation proposed by Kolakaluri [44] and the wetting of the particle surface was modeled according to Kariuki et al. [45]. Droplets that collide with apparatus walls are removed from the system. Water at 20 °C was assumed as spray medium with a Rosin–Rammler droplet size distribution. Injection position was matched to the tip of the nozzles and initial velocity was based on the spray air velocity during each run, respectively. Table 2 sums up the calibrated model parameters as well as the liquid and solid phase properties used for the simulations in this study.

3.1. Evaluation of liquid distribution

To analyze and quantify the distribution of the injected liquid within the fluidized bed, the injected droplets were tracked. For simplification, evaporation of droplets is not considered and every droplet that collides with a particle or the wall is assumed to be deposited there. Thus, rebound of droplets is neglected. The mass of liquid deposited on the particles in each cell is recorded as the deposition rate each second. Since the deposition rate in each individual cell is rather low, the simulated reactor volume is divided into twelve regions as shown in Fig. 2. In addition to the deposition rate field, the deposition rates over the whole volume of each of these regions was evaluated.

To additionally evaluate how efficiently the injected liquid was wetting the particles compared to the total injected fluid amount, the percentage of deposited and elutriated droplets as well as droplets colliding with the apparatus walls from the total injected liquid mass was calculated.

As reference case, a simulation of the prototype with 40° nozzle inclination and 0° nozzle position rotation is used. As process parameters, a spray rate of 80 g/min, spray air pressure of 1.75 bar, protection air pressure of 0.2 bar, and fluidization air flow of 130 m^3/h were set. In Fig. 3 the cumulative deposition rate throughout segments 1 and 2 of the fluidized bed at the end of the simulation time is visualized. To be able to see the deposition rates in the particle bed more clearly, slices of the field at 0.025 m vertical distance from one another are depicted up to a height of 0.2 m above the distributor. Furthermore, a threshold of 0.01 kg m^3_{cell}/s $m^3_{reactor}$ was applied to highlight the areas in which increased deposition occurs. To visualize the deposition rate field independently of the cell size, the deposited mass per second was multiplied by the cell volume and divided by the whole reactor volume.

In general, most particle–droplet collisions occur near the nozzle, where the droplets enter the particle bed. From this point, the spray zone expands in the direction, in which the nozzle is pointing. Moreover, a slight rotational shift of the deposition zone over the height of the prototype is visible, which is caused by the fluidization air flow that influences the droplets in addition to the nozzle air streams. Based on this depiction, the zone in which deposition occurs seems to be mostly similar in size and shape for both nozzles, indicating an overall even distribution of the injected liquid in the fluidized bed. However, slightly different expansions of the spray zone can be seen in both segments. While in segment 1, near the air inlet, the deposition rate is slightly further spread in vertical direction, in segment 2, the deposition rate is spread over a wider area in the horizontal plane. Due to the proximity of the first compartment to the fluidization air inlet, slightly higher gas velocities in this region might cause a longer flying distance of droplets before a collision with a particle occurs. For a better quantitative understanding of the liquid distribution, the deposition rate in the four lower segments (1 – 4 in Fig. 2) of the geometry is shown in Fig. 4.

Once liquid injection is started, the deposition rate in zones 1 and 2 quickly reaches a steady state at approximately 0.0045 kg/s. However, it has to be noted that this steady state only applies to the deposition rate and not necessarily other parameters, such as mixing of the phases in the fluidized bed. Both curves develop similarly over time and stay constant at about the same value confirming the overall even distribution of droplets as already assumed based on the visualization of the deposition rate field. Furthermore, this shows that the different expansion of the spray zone in front of both nozzles, as seen in Fig. 3, is minor. When taking the whole compartment into account, the spray distribution is nearly symmetrical. In the areas labeled 3 and 4 in Fig. 2 the deposition rate is significantly smaller with all values being below $5 \cdot 10^{-5}$ kg/s. Due to these small values the curves appear to be nearly overlapping in the diagram. Over the height of the reactor, the deposition rates decrease rapidly eventually reaching values below 10^{-6} kg/s in the upper half of the reactor. Consequently, at a bed mass of 3 kg, wetting of the particles predominantly happens in segments 1 and 2. Therefore, the discussion of the parameter study and geometric variations will be focused on the deposition rate in these segments. Overall, more than 90% of the injected droplets are deposited onto particles, thus being available for liquid bridging, less then 1% collide with the apparatus walls, and approximately 7% of the droplets are elutriated (see Section 3.2). In reality, those droplets would most likely be spray dried by the hot air stream and afterwards caught by the filters and returned into the fluidized bed as dust particles.

In addition to the deposition rate field shown in Fig. 3, Fig. 5 depicts several properties of the different phases at three different time points during simulation (2 s, 5 s, and 10 s after start). Near the nozzles, the air temperature is the lowest due to the colder air streams flowing through the nozzles in comparison to the fluidization air. This lower temperature zone is expanded throughout an overall stable volume with slight

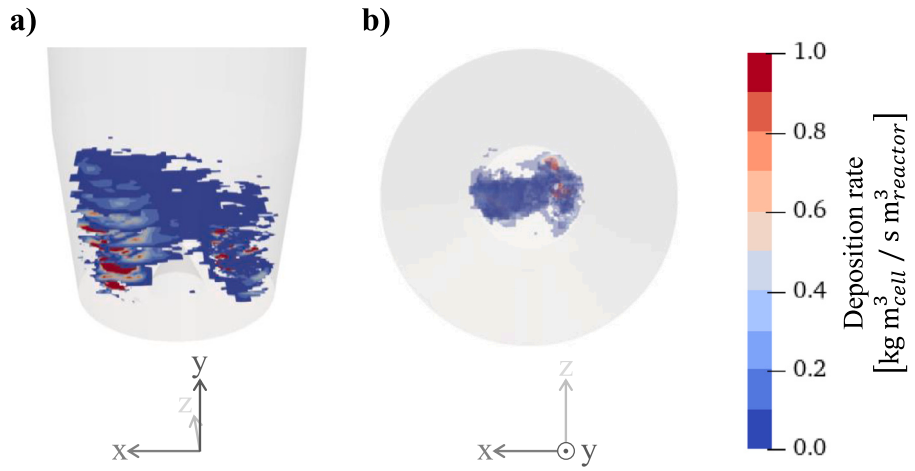

Fig. 3. Deposition rate after 10 s simulation time in prototype for reference case: (a) front view in X-Y plane, (b) top view in X-Z plane.

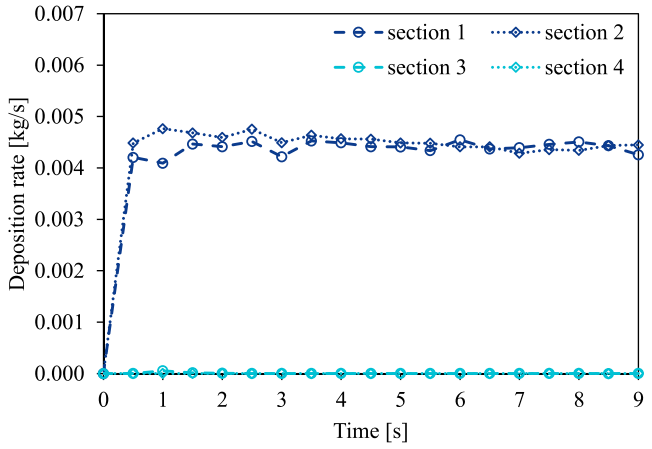

Fig. 4. Deposition rate over time in prototype for reference case in different segments of the reactor.

Table 3
Process parameters used in CFD-DEM simulations.

Parameter	Values	Unit
Liquid spray rate	40; 80; 120	g/min
Spray air pressure	0.5; 1.75; 3.0	bar
Protection air pressure	0.1; 0.2; 0.3	bar
Fluidization air volume flow	130; 200	m^3/h

Table 4
Fraction of deposited, elutriated, and wall droplets in prototype at different process parameters in comparison to reference case.

		Deposited droplets	Elutriated droplets	Droplets on wall
Reference case		93.2%	6.8%	$5.2 \cdot 10^{-3}$%
Liquid spray rate	40 g/min	93.2%	6.8%	$5.2 \cdot 10^{-3}$%
	120 g/min	94.1%	5.9%	$9.1 \cdot 10^{-3}$%
Spray air pressure	0.5 bar	92.0%	8.0%	$3.6 \cdot 10^{-3}$%
	3.0 bar	93.4%	6.6%	$3.6 \cdot 10^{-3}$%
Protection air pressure	0.1 bar	93.0%	7.0%	$4.4 \cdot 10^{-3}$%
	0.3 bar	93.3%	6.7%	$3.7 \cdot 10^{-3}$%
Fluidization air volume flow	200 m^3/h	84.5%	15.2%	$3.3 \cdot 10^{-1}$%

fluctuations. In Fig. 5b, the fluidization behavior of the particle bed can be observed based on the vertical velocity component of the particles. Lastly, the spray cone of the two nozzles and droplet size can be tracked in Fig. 5c. Due to the nature of the initial size distribution of the injected droplets, more droplets with a lower diameter can be observed.

3.2. Variation of process parameters

In order to analyze the liquid distribution at varied process conditions, four parameters connected to spray and fluidization behavior were changed: the liquid spray rate, the spray air pressure, the protection air pressure, and the fluidization air volume flow. Limits were chosen based on experimental studies to represent realistically applicable agglomeration conditions, yet cover a wide range for each parameter. A one-factor-at-a-time approach was used to keep the number of simulations and thus computational effort reasonable. The simulated process parameters are shown in Table 3. The standard nozzle inclination and position rotation chosen for the parameter study are 40° and 0°, respectively. Both nozzle air pressures are given as gauge pressures.

Table 4 provides an overview of the droplet fates after 10 s of simulated time at varied process parameters. As should be expected for an agglomeration process, most injected droplets, in most of the cases more than 90% are deposited on particles. At every simulated operating point, the fractions of droplets colliding with the apparatus wall is below 0.1%, showing that material loss due to wall deposition does not occur significantly in the prototype geometry over a broad range of process conditions. Still, it can be seen that more wall collisions occur at enhanced air pressures at the nozzles. Due to the inclination of the nozzles and the higher air velocities at the nozzle tip at these pressures, the droplets are accelerated faster towards the wall. A significant part of droplets, ranging between 6 and 12%, is elutriated from the system. Especially at high fluidization air flow, droplet elutriation is enhanced due to higher bed porosity and higher droplet acceleration.

For a more detailed analysis of the deposited droplets, Fig. 6 provides an overview of the deposition rates using the same settings as in Fig. 3. All fields were captured after 10 s simulation time (9 s after start of liquid injection) and depict the deposition rate in this time step. As expected, the deposition rate changes with varied spray and fluidization parameters. Out of the parameters investigated in this study, the spray rate has the most significant impact. When increasing the spray rate, the additional liquid injected per time step increases the deposition rate, which is the amount of droplets colliding with particles per second. The percentages of deposited, wall sticking, and elutriated droplets, however, are similar for all spray rates.

In Fig. 7, the deposition rate over time in the bottom segments (labeled 1 and 2 in Fig. 2) is shown for a spray rate of 40 g/min, 80 g/min, and 120 g/min and otherwise intermediate values of the remaining process parameters. Especially for the lower spray rate, the

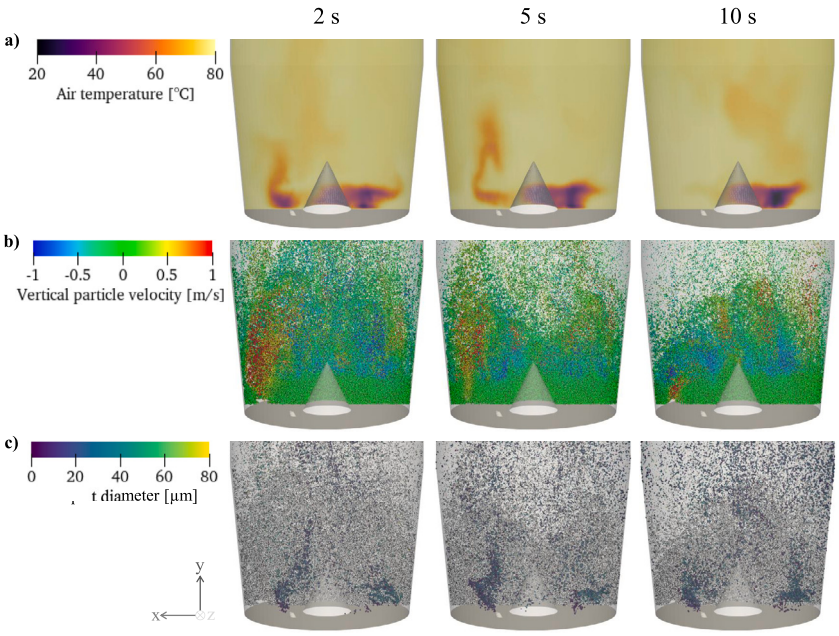

Fig. 5. Different phase properties over time in reference case: (a) air temperature, (b) vertical particle velocity, (c) droplet diameter (particles are shown in gray).

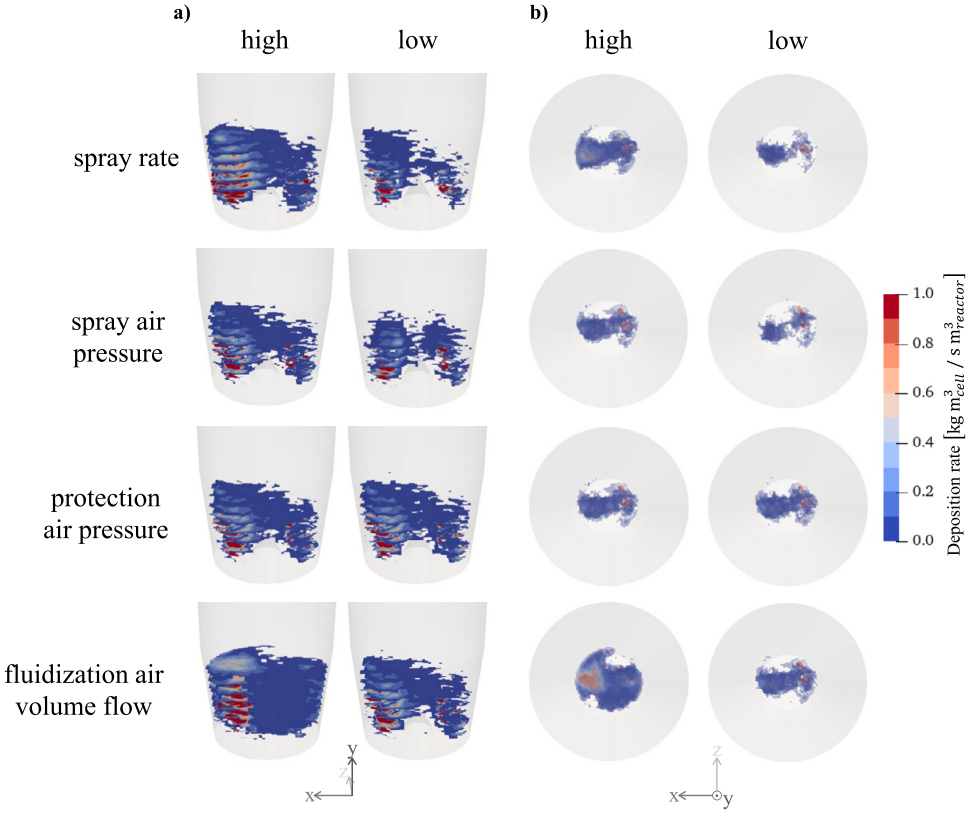

Fig. 6. Deposition rate after 10 s simulation time in prototype at different process parameters: (a) front view in X-Y plane, (b) top view in X-Z plane.

deposition rate is almost identical in both sections at a value just above 0.002 kg/s, which indicates that, despite of the tangential air inlet positioned at the edge of the wind box, a mostly evenly distributed fluidization air flow is created. In the beginning of the simulation with a higher spray rate, the deposition rate in the section near the fluidization air inlet lies slightly below the rate in the neighboring part. The increased number of droplets injected at 120 g/min and the accompanying enhanced number of particle–droplet collisions and wider distribution of particles through the fluidized bed can result in a higher fluctuation of the deposition rate compared to the run at a lower spray rate. Similar to the reference case slightly different expansions in vertical and horizontal direction can be seen in the two bottom segments in Fig. 6.

Figs. 8 and 9 depict the deposition rate in the lower reactor sections over a spray time of 9 s at different spray and protection air pressures, respectively. In general, the same effects on the droplet behavior can

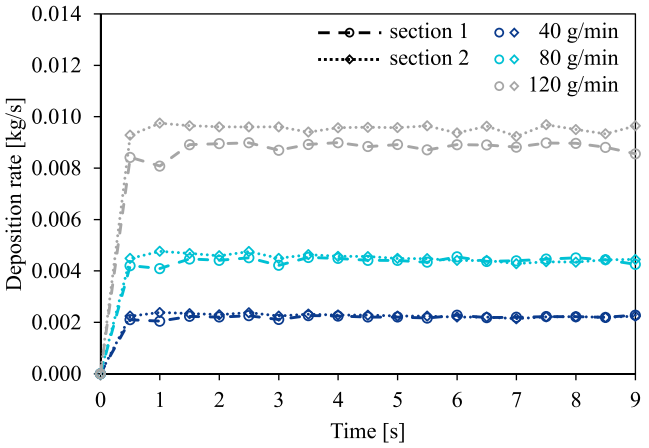

Fig. 7. Deposition rate over time in prototype at different spray rates.

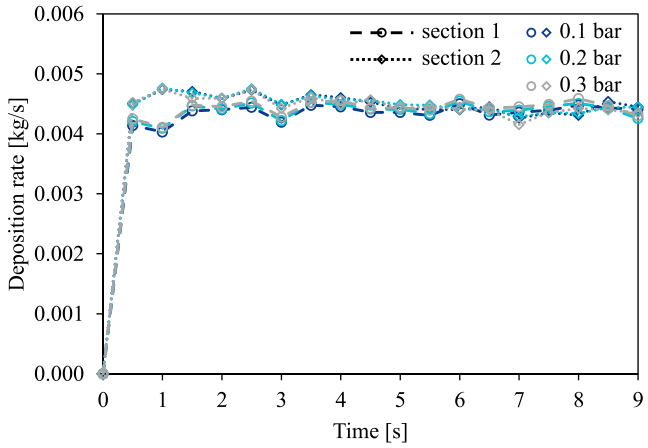

Fig. 9. Deposition rate over time in prototype at different protection air pressures.

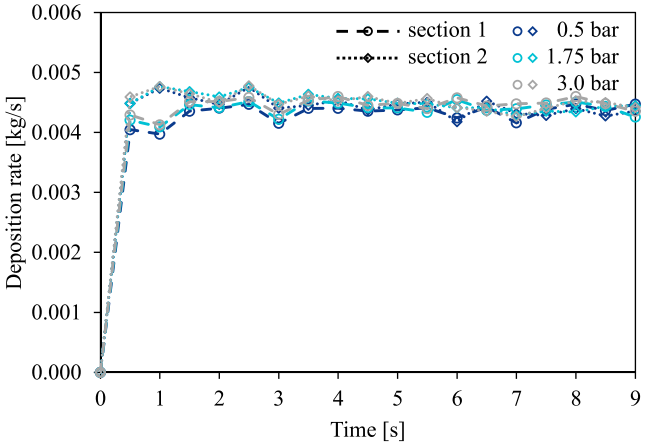

Fig. 8. Deposition rate over time in prototype at different spray air pressures.

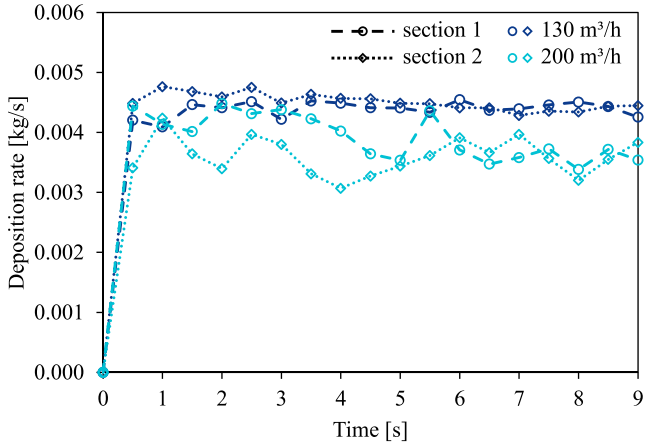

Fig. 10. Deposition rate over time in prototype at different fluidization air inlet volume flows.

be observed for both parameters. In both cases, the deposition rate is not largely affected by a change of pressure and is fluctuating around 0.004 kg/s. A slight increase in deposition rate can be seen at reduced nozzle pressures. In addition, increasing the spray and protection air pressures leads to a small raise of the percentage of elutriated droplets. Due to the elevated air velocities occurring at higher pressures, the liquid droplets are accelerated more, flying further upwards in the fluidized bed before colliding with a particle or flying through the whole bed getting elutriated. In addition, the solids-free zone in front of the nozzles expands since particles that move near the tip of a nozzle are also accelerated more by the faster nozzle air streams and fly further away into the fluidized bed.

Another gas stream that presumably influences the trajectories of the droplets and thus particle–droplet collisions, is the fluidization air. Fig. 10 shows the deposition rate in the bottom part of the fluidized bed at an inlet air flow rate of 130 m^3/h and 200 m^3/h. The corresponding superficial gas velocities above the distributor are 0.51 m/s and 0.79 m/s, respectively. At the elevated gas flow, the deposition rate in the two bottom parts of the fluidized bed is comparatively low since the droplets are entrained by the fluidization air. Thus, the droplets are dragged higher throughout the bed and travel at higher velocity, so the deposition rate in the upper segments of the fluidized bed is higher for an air flow of 200 m^3/h than for 130 m^3/h. In addition, the particle bed expands further at 200 m^3/h, which leads to an increased bed porosity and consequently reduces the probability of collisions between droplets and particles.

Table 5
Geometry modifications used in CFD-DEM simulations.

Parameter	Values	Unit
Nozzle inclination angle	40; 50; 60	°
Nozzle position rotation	0; 30; 45	°

3.3. Variation of reactor geometry

As previously mentioned, a great advantage of simulations compared to experiments is the possibility to investigate the effects of equipment modifications on the process without unreasonably high costs or effort. To optimize liquid distribution within the particle bed and minimize the number of droplets colliding with the reactor walls and being elutriated, the inclination angle of the two bottom-spray nozzles and the nozzle position relative to the fluidization air inlet were varied according to Table 5. For the latter, the setup as used for the parameter study is defined as “0°”. The further positions refer to a deviation from that position by moving both nozzles by a certain amount in circular direction. Lastly, the prototype geometry is compared to the commercially available fluidized bed setup *Solidlab 2* as described in Section 2.

Table 6 shows the percentages of deposited droplets, elutriated droplets and droplets colliding with the wall for different nozzle setups and reactor geometries. The most significant impact was observed due to the change from prototype to *Solidlab 2* geometry, where the fraction of deposited droplets was reduced by approximately 2%, which can be

Table 6
Fraction of deposited, elutriated, and wall droplets in modified prototype and *Solidlab 2* in comparison to reference case.

		Deposited droplets	Elutriated droplets	Droplets on wall
Reference case		93.2%	6.8%	$5.2 \cdot 10^{-3}$%
Nozzle inclination angle	50°	93.5%	6.5%	$2.9 \cdot 10^{-3}$%
	60°	91.5%	8.5%	$1.7 \cdot 10^{-3}$%
Nozzle position rotation	30°	93.5%	6.5%	$1.0 \cdot 10^{-2}$%
	45°	93.5%	6.5%	$2.0 \cdot 10^{-3}$%
Solidlab 2		91.3%	8.5%	$1.8 \cdot 10^{-1}$%

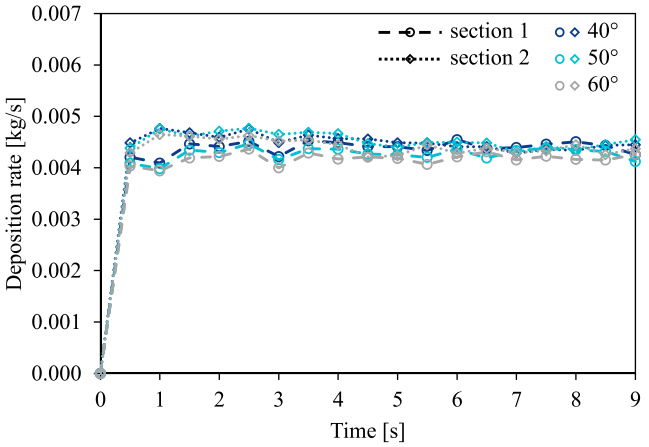

Fig. 11. Deposition rate over time at different nozzle inclination angles.

mostly attributed to an enhanced elutriation. Even though the fraction of droplets colliding with the wall is still the lowest, it is an order of magnitude higher in the *Solidlab 2* compared to the prototype. When comparing the different nozzle angles and positions in the prototype setup, only minimal differences in the percentages of various droplet fates can be detected. With higher inclination angle of the nozzles, more droplets are elutritated and less droplet–wall collisions occur since the nozzles are facing more towards the outlet and less towards the walls of the process chamber. Changing the position of the nozzles in the distributor plate did not affect the droplet fate significantly and the percentage of deposited droplets ranges between 93.2% and 93.5% for the three different positions. In the following, the deposited droplets in the different fluidized bed geometries will be discussed in more detail by evaluating the deposition rate in the bottom part of the fluidized bed.

Fig. 11 depicts the deposition rate over time in the bottom segments of the prototype geometry at different inclination angles of the two bottom spray nozzles. With increasing angle the deposition rate slightly decreases due to the more upwards facing nozzles favoring elutriation, which is also evident in the percentage of elutriated droplets in Table 6. The initial goal to minimize droplet-wall collisions by increasing the nozzle angle was achieved. However, since the fraction of droplets sticking to the wall is significantly lower compared to the deposited and elutriated droplets, the effect is neglectable. In general, all three nozzle setups show a mostly similar behavior with only minor differences, regarding both, the overall distribution of droplet fates as well as the deposition rate. This indicates that for a sufficiently large bed height, the nozzle inclination angle can be varied within a certain range in order to accommodate to possible external geometric constraints without significantly affecting the liquid distribution and thus the product quality. Still, at lower bed masses, the risk of spraying droplets out of the fluidized bed at steep nozzle angles should be considered.

The effect of the second geometric adaptation, the variation of the nozzle position, on the deposition rate is shown in Fig. 12. As in the

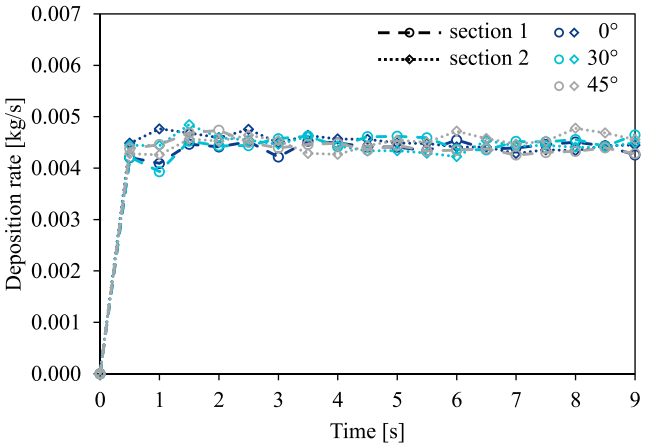

Fig. 12. Deposition rate over time at different nozzle position rotation.

other simulation cases considered so far, the deposition rate reaches a steady state almost immediately after liquid injection is started. Just as for the nozzle inclination angle, the deposition rate does not seem to be significantly affected by rotating the position of the nozzles along the distributor. Consequently, this enables further possible geometry modifications to meet external requirements without impairing product quality. Moreover, it can be concluded that the incoming fluidization air is evenly distributed over the whole cross-section of the apparatus by combining the tangential air inlet with the inclined slits of the *Diskjet* distributor.

Some significant changes in the apparatus design are apparent when comparing the prototype to the *Solidlab 2*. One major difference is the fluidization air inlet which is installed tangentially in case of the prototype and centrally for the *Solidlab 2*. Fig. 13 shows slices of the deposition rate field in the *Solidlab 2* after 10 s. Just as for the prototype, the majority of particle–droplet collisions occurs just in front of the nozzles. However, the overall shape of the spray zone characterized by the deposition rate field is different for both geometries. In the *Solidlab 2*, the spray zones from both nozzles are broader and merge into one large zone approximately 0.1 m above the distributor. Furthermore, the spray zone expands up to the reactor wall in certain parts of the fluidized bed, while it does not reach the wall on the left side of the air inlet.

The deposition rate in the bottom part of both granulators over time is shown in Fig. 14. In the first two seconds, the deposition rate in the *Solidlab 2* is lower than the rate in the prototype, which means that less collisions between particles and droplets occur. Afterwards, the deposition rate in the *Solidlab 2* increases up to 0.005 kg/s, which is higher than in the prototype. However, the *Solidlab 2* curve shows higher fluctuations and overall seems to be slightly less stable in comparison to the state of the prototype. In addition, a higher difference between the deposition rate in segment 1 and 2 can be observed, indicating a less symmetrical distribution of the liquid within the fluidized bed. Therefore, the deposition of liquid droplets onto the particles of the fluidized bed should happen more uniformly in the prototype granulator which can be attributed to a more even distribution of the fluidization air allowing an overall better fluidization of the particle bed and enhanced interaction between particles and injected droplets.

4. Conclusion

To investigate the distribution of an injected liquid in a fluidized bed and thus contribute to better understand the agglomeration process, CFD-DEM simulations were performed. Furthermore, a procedure to analyze where droplets and particles interact with each other and what percentage of the injected liquid contributes to agglomeration

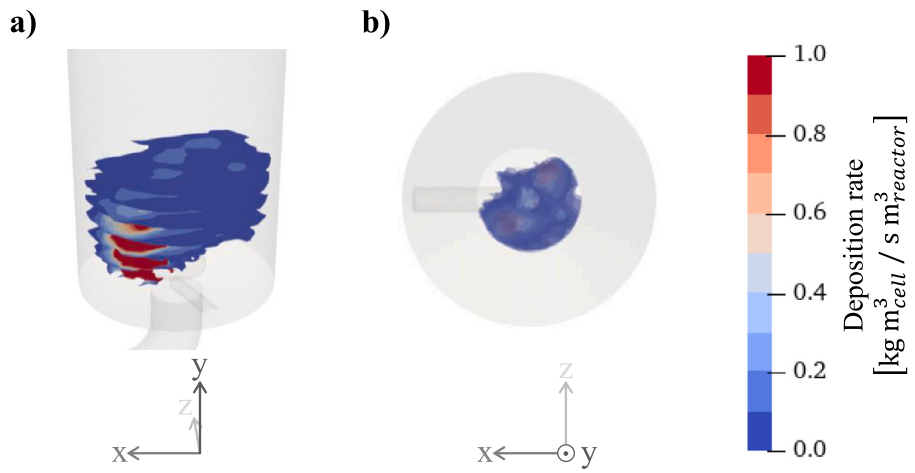

Fig. 13. Deposition rate after 10 s simulation time in *Solidlab 2*: (a) front view in X-Y plane, (b) top view in X-Z plane.

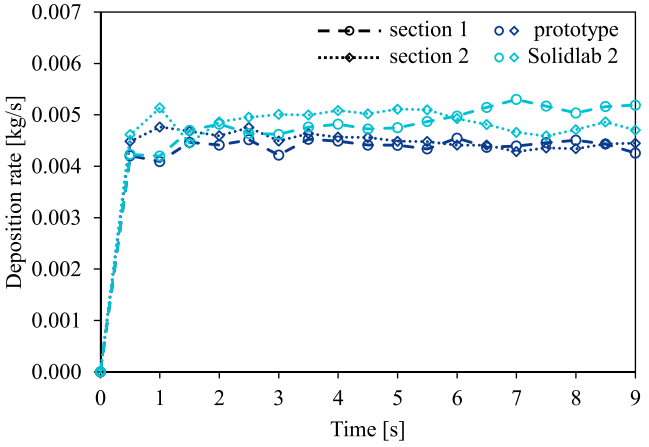

Fig. 14. Deposition rate over time for prototype reference case and *Solidlab 2*.

by being available on the particle surface for the formation of liquid bridges was established. For industrial processes this knowledge is extremely valuable to evaluate process efficiency and consequently optimize the agglomeration by minimizing the amount of droplets that do not contribute to particle growth due to elutriation or collision with the reactor walls. Furthermore, an even liquid distribution contributes to a uniform product quality, thus also providing helpful information with regard to process design.

Overall, a steady deposition rate with slight fluctuations was reached in all investigated cases. In the bottom segments of the fluidized bed, where a majority of the particle–droplet collisions occur, a mostly similar distribution of the droplets injected by the two bottom spray nozzles was observed. While increasing the liquid spray rate naturally lead to a higher deposition rate, the percentages of deposited, wall-sticking, and elutriated droplets were not affected. In contrast, an increase in spray and protection air pressure mainly influenced the amount of droplets on the wall and in the filters and only has a minor impact on the deposition rate in the lower part of the fluidized bed. A higher fluidization air volume flow caused a lower deposition rate in the bottom segments and enhances elutriation due to the increased acceleration of the injected droplets and higher bed porosity.

Even when varying the inclination and position of the bottom-spray nozzles, the liquid distribution characterized by the deposition rate, could be maintained. Therefore, a versatile setup of the prototype geometry, that can meet external requirements, e.g. concerning spacial limitations, without loss of product quality, is possible. A tangential inlet for the fluidization air was found to be favorable for the investigated process with regard to a uniform deposition of droplets in comparison to a central gas inlet.

CRediT authorship contribution statement

Maike Orth: Writing – original draft, Visualization, Validation, Formal analysis, Data curation, Conceptualization. **Aitor Atxutegi:** Writing – review & editing, Validation, Software, Methodology, Formal analysis, Conceptualization. **Matthias Börner:** Writing – review & editing, Visualization, Supervision, Project administration, Conceptualization. **Swantje Pietsch-Braune:** Writing – review & editing, Supervision, Project administration. **Stefan Heinrich:** Writing – review & editing, Supervision, Resources, Project administration, Funding acquisition.

Declaration of competing interest

The authors declare that they have no known competing financial interests or personal relationships that could have appeared to influence the work reported in this paper.

Data availability

Data will be made available on request.

Acknowledgment

This work was supported by Syntegon Technology.

References

[1] D.E. Wurster, Air-suspension technique of coating drug particles, J. Am. Pharm. Assoc. 48 (8) (1959) 451–454.
[2] R. Boerefijn, M.J. Hounslow, Studies of fluid bed granulation in an industrial R&D context, Chem. Eng. Sci. 60 (14) (2005) 3879–3890, http://dx.doi.org/10.1016/j.ces.2005.02.021.
[3] G.K. Reynolds, J.S. Fu, Y.S. Cheong, M.J. Hounslow, A.D. Salman, Breakage in granulation: A review, Chem. Eng. Sci. 60 (14) (2005) 3969–3992, http://dx.doi.org/10.1016/j.ces.2005.02.029.
[4] B.J. Ennis, J.D. Litster, Particle size enlargement, in: D.W. Green, M.Z. Southard (Eds.), Perry's Chemical Engineers' Handbook, McGraw-Hill Education, New York, 2019, 20–56–20–89.
[5] S.M. Iveson, J.D. Litster, K. Hapgood, B.J. Ennis, Nucleation, growth and breakage phenomena in agitated wet granulation processes: a review, Powder Technol. 117 (1–2) (2001) 3–39, http://dx.doi.org/10.1016/S0032-5910(01)00313-8.
[6] H. Uhlemann, L. Mörl, Wirbelschicht-Sprühgranulation, VDI-Buch, Springer, Berlin and Heidelberg, 2000.
[7] M. Hemati, R. Cherif, K. Saleh, V. Pont, Fluidized bed coating and granulation: influence of process-related variables and physicochemical properties on the growth kinetics, Powder Technol. 130 (1–3) (2003) 18–34, http://dx.doi.org/10.1016/S0032-5910(02)00221-8.

[8] V. Pont, K. Saleh, D. Steinmetz, M. Hemati, Influence of the physicochemical properties on the growth of solid particles by granulation in fluidized bed, Powder Technol. 120 (1–2) (2001) 97–104, http://dx.doi.org/10.1016/S0032-5910(01)00355-2.
[9] P. Rajniak, C. Mancinelli, R.T. Chern, F. Stepanek, L. Farber, B.T. Hill, Experimental study of wet granulation in fluidized bed: impact of the binder properties on the granule morphology, Int. J. Pharmaceut. 334 (1–2) (2007) 92–102, http://dx.doi.org/10.1016/j.ijpharm.2006.10.040.
[10] J. Bouffard, M. Kaster, H. Dumont, Influence of process variable and physicochemical properties on the granulation mechanism of mannitol in a fluid bed top spray granulator, Drug Dev. Ind. Pharm. 31 (9) (2005) 923–933, http://dx.doi.org/10.1080/03639040500272124.
[11] M. Dadkhah, E. Tsotsas, Influence of process variables on internal particle structure in spray fluidized bed agglomeration, Powder Technol. 258 (2014) 165–173, http://dx.doi.org/10.1016/j.powtec.2014.03.005.
[12] D.M. Lipps, A.M. Sakr, Characterization of wet granulation process parameters using response surface methodology. 1. Top-spray fluidized bed, J. Pharm. Sci. 83 (7) (1994) 937–947, http://dx.doi.org/10.1002/jps.2600830705.
[13] K. Saleh, R. Cherif, M. Hemati, An experimental study of fluidized-bed coating: influence of operating conditions on growth rate and mechanism, Adv. Powder Technol. 10 (3) (1999) 255–277, http://dx.doi.org/10.1163/156855299X00334.
[14] U. Vengateson, R. Mohan, Experimental and modeling study of fluidized bed granulation: Effect of binder flow rate and fluidizing air velocity, Resour.-Effic. Technol. 2 (2016) S124–S135, http://dx.doi.org/10.1016/j.reffit.2016.10.003.
[15] L. Fries, Discrete Particle Modeling of a Fluidized Bed Granulator (Dissertation), Hamburg University of Technology, Hamburg, 2012.
[16] K.C. Link, E.-U. Schlünder, Fluidized bed spray granulation, Chem. Eng. Process.: Process Intensif. 36 (6) (1997) 443–457, http://dx.doi.org/10.1016/S0255-2701(97)00022-6.
[17] F. Ronsse, J.G. Pieters, K. Dewettinck, Modelling side-effect spray drying in top-spray fluidised bed coating processes, J. Food Eng. 86 (4) (2008) 529–541, http://dx.doi.org/10.1016/j.jfoodeng.2007.11.003.
[18] E.S.K. Tang, L. Wang, C.V. Liew, L.W. Chan, P.W.S. Heng, Drying efficiency and particle movement in coating–impact on particle agglomeration and yield, Int. J. Pharmaceut. 350 (1–2) (2008) 172–180, http://dx.doi.org/10.1016/j.ijpharm.2007.08.047.
[19] S. Karlsson, A. Rasmuson, B. van Wachem, I.N. Björn, CFD modeling of the Wurster bed coater, AIChE J. 55 (10) (2009) 2578–2590, http://dx.doi.org/10.1002/aic.11847.
[20] S.R.L. Werner, J.R. Jones, A.H.J. Paterson, R.H. Archer, D.L. Pearce, Air-suspension coating in the food industry: Part II — micro-level process approach, Powder Technol. 171 (1) (2007) 34–45, http://dx.doi.org/10.1016/j.powtec.2006.08.015.
[21] R. Turton, Challenges in the modeling and prediction of coating of pharmaceutical dosage forms, Powder Technol. 181 (2) (2008) 186–194, http://dx.doi.org/10.1016/j.powtec.2006.12.006.
[22] I.T. Cameron, F.Y. Wang, C.D. Immanuel, F. Stepanek, Process systems modelling and applications in granulation: A review, Chem. Eng. Sci. 60 (14) (2005) 3723–3750, http://dx.doi.org/10.1016/j.ces.2005.02.004.
[23] M. Singh, S. Shirazian, V. Ranade, G.M. Walker, A. Kumar, Challenges and opportunities in modelling wet granulation in pharmaceutical industry – A critical review, Powder Technol. 403 (2022) 117380, http://dx.doi.org/10.1016/j.powtec.2022.117380.
[24] Y. Tsuji, T. Kawaguchi, T. Tanaka, Discrete particle simulation of two-dimensional fluidized bed, Powder Technol. 77 (1) (1993) 79–87, http://dx.doi.org/10.1016/0032-5910(93)85010-7.
[25] P. Kieckhefen, S. Pietsch, M. Dosta, S. Heinrich, Possibilities and limits of computational fluid dynamics-discrete element method simulations in process engineering: A review of recent advancements and future trends, Annu. Rev. Chem. Biomol. Eng. 11 (2020) 397–422, http://dx.doi.org/10.1146/annurev-chembioeng-110519-075414.
[26] M.J.V. Goldschmidt, G.G.C. Weijers, R. Boerefijn, J.A.M. Kuipers, Discrete element modelling of fluidised bed spray granulation, Powder Technol. 138 (1) (2003) 39–45, http://dx.doi.org/10.1016/j.powtec.2003.08.045.
[27] J.M. Link, W. Godlieb, N.G. Deen, J.A.M. Kuipers, Discrete element study of granulation in a spout-fluidized bed, Chem. Eng. Sci. 62 (1–2) (2007) 195–207, http://dx.doi.org/10.1016/j.ces.2006.08.018.
[28] M.S. van Buijtenen, N.G. Deen, S. Heinrich, S. Antonyuk, J.A.M. Kuipers, A discrete element study of wet particle–particle interaction during granulation in a spout fluidized bed, Can. J. Chem. Eng. 87 (2) (2009) 308–317, http://dx.doi.org/10.1002/cjce.20144.
[29] V.S. Sutkar, N.G. Deen, A.V. Patil, V. Salikov, S. Antonyuk, S. Heinrich, J.A.M. Kuipers, CFD–DEM model for coupled heat and mass transfer in a spout fluidized bed with liquid injection, Chem. Eng. J. 288 (2016) 185–197, http://dx.doi.org/10.1016/j.cej.2015.11.044.
[30] D.K. Kafui, C. Thornton, Fully-3D DEM simulation of fluidised bed spray granulation using an exploratory surface energy-based spray zone concept, Powder Technol. 184 (2) (2008) 177–188, http://dx.doi.org/10.1016/j.powtec.2007.11.038.
[31] L. Fries, S. Antonyuk, S. Heinrich, S. Palzer, DEM-CFD modeling of a fluidized bed spray granulator, Chem. Eng. Sci. 66 (11) (2011) 2340–2355, http://dx.doi.org/10.1016/j.ces.2011.02.038.
[32] L. Fries, M. Dosta, S. Antonyuk, S. Heinrich, S. Palzer, Moisture distribution in fluidized beds with liquid injection, Chem. Eng. Technol. 34 (7) (2011) 1076–1084, http://dx.doi.org/10.1002/ceat.201100132.
[33] L. Fries, S. Antonyuk, S. Heinrich, D. Dopfer, S. Palzer, Collision dynamics in fluidised bed granulators: A DEM-CFD study, Chem. Eng. Sci. 86 (2013) 108–123, http://dx.doi.org/10.1016/j.ces.2012.06.026.
[34] M. Börner, A. Bück, E. Tsotsas, DEM-CFD investigation of particle residence time distribution in top-spray fluidised bed granulation, Chem. Eng. Sci. 161 (2017) 187–197, http://dx.doi.org/10.1016/j.ces.2016.12.020.
[35] P. Kieckhefen, A Novel Method for Predicting Product Properties in Fluidized Bed Spray Granulation (Dissertation), Hamburg University of Technology, Hamburg, 2021.
[36] H.G. Weller, G. Tabor, H. Jasak, C. Fureby, A tensorial approach to computational continuum mechanics using object-oriented techniques, Comput. Phys. 12 (6) (1998) 620–631, http://dx.doi.org/10.1063/1.168744.
[37] C. Kloss, C. Goniva, A. Hager, S. Amberger, S. Pirker, Models, algorithms and validation for opensource DEM and CFD-DEM, Prog. Comput. Fluid Dyn. Int. J. 12 (2/3) (2012) 140, http://dx.doi.org/10.1504/PCFD.2012.047457.
[38] C. Goniva, C. Kloss, N.G. Deen, J.A.M. Kuipers, S. Pirker, Influence of rolling friction on single spout fluidized bed simulation, Particuology 10 (5) (2012) 582–591, http://dx.doi.org/10.1016/j.partic.2012.05.002.
[39] R. Beetstra, M.A. van der Hoef, J.A.M. Kuipers, Drag force of intermediate Reynolds number flow past mono– and bidisperse arrays of spheres, AIChE J. 53 (2) (2007) 489–501, http://dx.doi.org/10.1002/aic.11065.
[40] A. Di Renzo, F.P. Di Maio, Comparison of contact-force models for the simulation of collisions in DEM-based granular flow codes, Chem. Eng. Sci. 59 (3) (2004) 525–541, http://dx.doi.org/10.1016/j.ces.2003.09.037.
[41] P. Kieckhefen, S. Pietsch, M. Höfert, M. Schönherr, S. Heinrich, F. Kleine Jäger, Influence of gas inflow modelling on CFD-DEM simulations of three-dimensional prismatic spouted beds, Powder Technol. 329 (2018) 167–180, http://dx.doi.org/10.1016/j.powtec.2018.01.048.
[42] C. Bierwisch, T. Kraft, H. Riedel, M. Moseler, Three-dimensional discrete element models for the granular statics and dynamics of powders in cavity filling, J. Mech. Phys. Solids 57 (1) (2009) 10–31, http://dx.doi.org/10.1016/j.jmps.2008.10.006.
[43] P. Kieckhefen, T. Lichtenegger, S. Pietsch, S. Pirker, S. Heinrich, Simulation of spray coating in a spouted bed using recurrence CFD, Particuology 42 (2019) 92–103, http://dx.doi.org/10.1016/j.partic.2018.01.008.
[44] R. Kolakaluri, Direct Numerical Simulations and Analytical Modeling of Granular Filtration (Dissertation), Iowa State University, Ames, 2013.
[45] W.I.J. Kariuki, B. Freireich, R.M. Smith, M. Rhodes, K.P. Hapgood, Distribution nucleation: Quantifying liquid distribution on the particle surface using the dimensionless particle coating number, Chem. Eng. Sci. 92 (2013) 134–145, http://dx.doi.org/10.1016/j.ces.2013.01.010.

Maike Orth is a doctoral student at the Institute of Solid Process Engineering and Particle Technology at the Hamburg University of Technology. There, she obtained a M.Sc. in Process Engineering with distinction in 2019. Her research interests include particle formulation in fluidized beds, particle characterization, and CFD-DEM simulations of fluidized bed processes.

Dr. Aitor Atxutegi studied Chemical Engineering and obtained his doctoral degree in 2020 under the supervision of Prof. Olazar at University of the Basque Country (EHU/UPV) with a clear focus on CFD-DEM simulation and experimental PTV validation of the fluidization of irregular particles in conical spouted beds with internal devices. Since 2021 he is working as a group leader at TUHH in the experimental and simulation of granulators with special emphasis on improving the process control through simulation predictive techniques and the implementation of coating models for tablet homogeneity prediction.

Dr.-Ing. Matthias Börner is heading the research and development department at a Syntegon site in Schopfheim, Germany. Syntegon is an equipment manufacturer of fluid bed and mixer technology for the pharmaceutical industry. Matthias Börner studied process engineering at the University of Magdeburg until 2008. After his studies he obtained a Ph.D. in 2013 about CFDDEM simulations and experimental flow characterizations in fluid bed granulation equipment.

Dr.-Ing. Swantje Pietsch-Braune is a senior engineer in the Institute of Solids Process Engineering and Particle Technology at Hamburg University of Technology. She obtained her Ph.D. in 2018 on the experimental and numerical investigations of fluidization behavior and liquid injection in three-dimensional prismatic spouted

beds. Her research is focused on particle formulation in fluidized beds and CFD-DEM simulations of these processes.

Prof. Dr.-Ing. Stefan Heinrich obtained his diploma in Process Engineering and a doctoral degree at the University Magdeburg. After positions as Assistant and Junior Professor and a Habilitation, he became full professor at the TUHH and director of the Institute of Solids Process Engineering and Particle Technology in 2008. He is editor of Advanced Powder Technology and Particuology, chairman of the Working Party on Agglomeration and Bulk Solids Technology of VDI-ProcessNet and of the EFCE Working Party on Agglomeration. His main research interests are fluidized bed technology, mainly for drying and particle formulation, particle simulation methods as well as contact, deformation and breakage mechanics of particles. He received the DECHEMA-Prize 2015.